JACS
JOURNAL OF THE AMERICAN CHEMICAL SOCIETY
Article
pubs.acs.org/JACS

Decomposition of Condensed Phase Energetic Materials: Interplay between Uni- and Bimolecular Mechanisms

David Furman,*[,†,∥] Ronnie Kosloff,[†] Faina Dubnikova,[†] Sergey V. Zybin,[‡] William A. Goddard, III,[‡] Naomi Rom,[†] Barak Hirshberg,[†] and Yehuda Zeiri[§,∥]

[†]Fritz Haber Research Center for Molecular Dynamics, Institute of Chemistry, The Hebrew University of Jerusalem, Jerusalem 91904, Israel

[‡]Materials and Process Simulation Center, California Institute of Technology, Pasadena, California 91125, United States

[§]Biomedical Engineering, Ben Gurion University, Beer-Sheva 94105, Israel

[∥]Division of Chemistry, NRCN, P.O. Box 9001, Beer-Sheva 84190, Israel

Supporting Information

ABSTRACT: Activation energy for the decomposition of explosives is a crucial parameter of performance. The dramatic suppression of activation energy in condensed phase decomposition of nitroaromatic explosives has been an unresolved issue for over a decade. We rationalize the reduction in activation energy as a result of a mechanistic change from unimolecular decomposition in the gas phase to a series of radical bimolecular reactions in the condensed phase. This is in contrast to other classes of explosives, such as nitramines and nitrate esters, whose decomposition proceeds via unimolecular reactions both in the gas and in the condensed phase. The thermal decomposition of a model nitroaromatic explosive, 2,4,6-trinitrotoluene (TNT), is presented as a prime example. Electronic structure and reactive molecular dynamics (ReaxFF-*lg*) calculations enable to directly probe the condensed phase chemistry under extreme conditions of temperature and pressure, identifying the key bimolecular radical reactions responsible for the low activation route. This study elucidates the origin of the difference between the activation energies in the gas phase (~62 kcal/mol) and the condensed phase (~35 kcal/mol) of TNT and identifies the corresponding universal principle. On the basis of these findings, the different reactivities of nitro-based organic explosives are rationalized as an interplay between uni- and bimolecular processes.

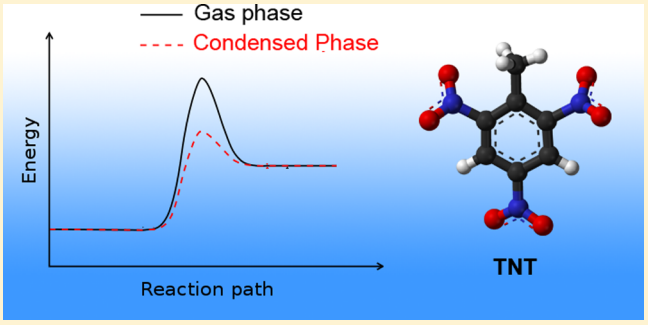

1. INTRODUCTION

The physical and chemical events that occur in condensed phase explosive devices under extreme conditions are a subject of great importance traditionally driven by the defense communities. Elevated pressure and temperature conditions as found within detonating explosives offer exciting applications in many fields, including large scale production of nano-diamonds,[1,2] advanced energy generation,[3] and chemistry of planetary interiors.[4] Unfortunately, despite decades of research, the microscopic details of initiation and detonation of energetic materials remain unclear. The experimental determination of kinetic parameters and time-resolved mechanism pathways is particularly challenging for condensed phase systems, where multimolecular decomposition channels may be present in addition to complicated homogeneous and heterogeneous catalysis effects.[5−7]

The decomposition of some high explosives is known to be pressure dependent,[8−10] thus one should expect noticeable differences between the gas pahse and condensed phase systems. In this respect, it is intriguing that some types of explosives show no difference in activation energy, whereas others decompose up to 10 times faster in the condensed phase.[7] For example, TNT and TATB have considerably lower activation energies in the condensed phase as can be seen in Table 1, while the group of nonaromatic explosives is characterized by a similar value in both phases. Surprisingly, the nitroaromatic explosive 1,3,5-trinitrobenzene (TNB) shows the same trend as RDX, PETN, and HMX.

Explosives decompose by a branching chain of radical reactions. The rate-determining step is associated with the first bottleneck in the decomposition pathway. In gas phase nitro-based explosives the activation energy is determined by the unimolecular NO_2 cleavage. In condensed phase, the appearance of NO_2 signals that the activation barrier has been overcome. However, in contrast to the gas phase, the route leading to NO_2 cleavage goes through a series of radical mediated bimolecular reactions. The activation energy of the bimolecular pathway is therefore determined by the highest barrier in the sequence. For this pathway to dominate in the

Received: October 4, 2013
Published: February 4, 2014

   dx.doi.org/10.1021/ja410020f | *J. Am. Chem. Soc.* 2014, 136, 4192−4200

Table 1. Global Activation Energies of Condensed Phase Nitroaromatic, Nitramine and Nitrate Ester High Explosives and Unimolecular DFT Energy Barriers for NO_2 Cleavage

family	nonaromatic			aromatic		
$\Delta E^{\ddagger}$ (kcal/mol)	HMX	PETN	RDX	TNB	TNT	TATB
gas phase DFT results	42.8[12]	46.5	41.5	64.0,[11] 67.7[13]	61.7	69.4,[11] 77.2[12]
condensed phase experimental results	48.47;[23] 52.7[24]	41.83−62.86[21,22]	47.1,[16] 53.6[20]	67.3 ± 0.8[19]	34.4,[6] 43.4,[17] 41.4[18]	60.0;[14] 59.1;[15] 42.0[16]
$\Delta(\Delta E^{\ddagger})$	−5.5	−5.8	−8.8	−1.45	+21.8	+19.6

condensed phase, the bimolecular barrier should be lower than the unimolecular barrier. This thesis is employed in the present study to classify the nitro-based explosives with respect to their decomposition mechanism.

It was proposed that intermolecular hydrogen transfer is the first step of decomposition of molten TNT. On the other hand, in nitrate esters and nitramines, the decomposition in the gas phase is faster than in condensed phase, supporting a unimolecular decomposition mechanism.[19,7] In other aromatic compounds, in a series of isothermal decomposition studies in dilute supercritical solutions, Minier et al.[25] found that the rate-controlling step for nitrobenzene and *p*-nitrotoluene is probably intermolecular hydrogen transfer from solvent molecules. A bimolecular path is also supported by Davis et al.[26] with evidence of intermolecular hydrogen transfer reactions for shock-induced reactions in nitroaromatic compounds in the gas phase at high pressures. However, this contradicts the studies of Brill and James[19,27] and others[28,29] claiming that the dominant rate-controlling step in nitroaromatic explosives is a unimolecular C-NO_2 homolysis reaction.

To provide detailed mechanistic insight with an atomistic resolution into the decomposition of condensed phase explosives, we present the results of comprehensive reactive molecular dynamics and electronic structure calculations. The present study focuses on nitroaromatic compounds, such as TNT as a prime example, but has straightforward implications to other nitroaromatic explosives, such as TNB and 1,3,5-triamino-2,4,6-trinitrobenzene (TATB). A unit cell and a super cell of TNT used in the study are illustrated in Figure 1. The

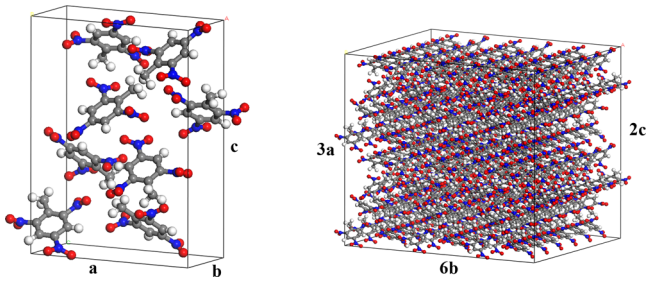

Figure 1. (left) Experimental unit cell and lattice vectors of *o*-2,4,6-trinitrotoluene (a = 14.91 Å, b = 6.03 Å, c = 19.68 Å) and (right) noncompressed super cell consisting of 288 molecules.

simulations allow us to directly sample an isothermal system by maintaining a constant target temperature. It should be mentioned that our simulations avoid the preceding step of compression and heating caused by the shock wave, but by employing broad ranges of temperature and initial material compression (1800−3500 K and 0−30% volumetric compression) we gain insight into the complex set of physical and chemical processes occurring at these extreme conditions at the Chapman−Jouguet state during detonation. We present a new bimolecular assisted channel leading to the enhanced formation of the NO_2 intermediate at a highly reduced cost compared to gas phase formation, in agreement with the contradictory experimental observations. The results are compared to previously published[30] and new DFT calculations.

In the following the paper is thus organized: Section 2 describes the technical details of the various computational methods used in this study. Section 3 is devoted to a short description of the decomposition mechanisms in the gas phase, followed by a detailed description of the initial steps of decomposition in the condensed phase as revealed by ReaxFF-*lg* simulations. Section 4 presents an analysis of final decomposition products. Section 5 presents a description of the thermodynamics and kinetics of the thermal decomposition process, followed by Section 6 which provides an elucidation of the governing mechanism of condensed phase nitroaromatic explosives. Finally, Section 7 provides a short summary of main results and conclusions.

2. COMPUTATIONAL DETAILS

2.1. ReaxFF-*lg* Reactive Force Field. The reactive force field ReaxFF-*lg*[31] partitions the system energy into a sum of contributions as shown in eq 1

$$E_{\text{system}} = E_{\text{bond}} + E_{\text{lp}} + E_{\text{over}} + E_{\text{under}} + E_{\text{val}} + E_{\text{pen}} + E_{\text{tors}} + E_{\text{conj}} + E_{\text{H-bond}} + E_{\text{vdW}} + E_{\text{Coulomb}} + E_{\text{lg}} \quad (1)$$

Generally, the total energy of the system consists of three types: covalent bond order-dependent terms (bonds, angles and torsions), electrostatic forces and van der Waals interactions between all atomic pairs.[31] The covalent part is mainly responsible for the reactivity of the force field, describing instantaneous bond formation and rupture events as smooth functions of the interatomic separations for σ, π, and $\pi\pi$ bonds.

$$\mathrm{BO}'_{ij} = \mathrm{BO}^{\sigma}_{ij} + \mathrm{BO}^{\pi}_{ij} + \mathrm{BO}^{\pi\pi}_{ij} = \exp\left[p_{\text{bo1}}\left(\frac{r_{ij}}{r^{\sigma}_{0}}\right)^{p_{\text{bo2}}}\right] + \exp\left[p_{\text{bo3}}\left(\frac{r_{ij}}{r^{\pi}_{0}}\right)^{p_{\text{bo4}}}\right] + \exp\left[p_{\text{bo5}}\left(\frac{r_{ij}}{r^{\pi\pi}_{0}}\right)^{p_{\text{bo6}}}\right] \quad (2)$$

The bond order, BO'_{ij}, in eq 2 is calculated on-the-fly and consecutively corrected with under- and overcoordination terms to attain the correct valency. In addition, ReaxFF-*lg* accounts for polarization effects by using a geometry-dependent charge equilibration scheme. All parameters are optimized to reproduce QM data. In the present study the nitramines-trained force field was used with low gradient correction for dispersion interactions. The long-range correction factor is responsible for a proper description of vdW and London forces between molecules and has been shown to be important in molecular solids. The parametrization is based on a large number of ab initio QM calculations of nitramine and nitroaromatic high energy compounds both at ambient and at extreme conditions.[8,32−34]

We briefly describe the correction method presented extensively elsewhere.[31] The proposed method adds a correction factor to the original ReaxFF total energy expression[35] (eq 1) in order to keep the fitted parameters intact, while adding the capability to train a new set of correction parameters so as to predict the correct density and heat

dx.doi.org/10.1021/ja410020f | J. Am. Chem. Soc. 2014, 136, 4192−4200

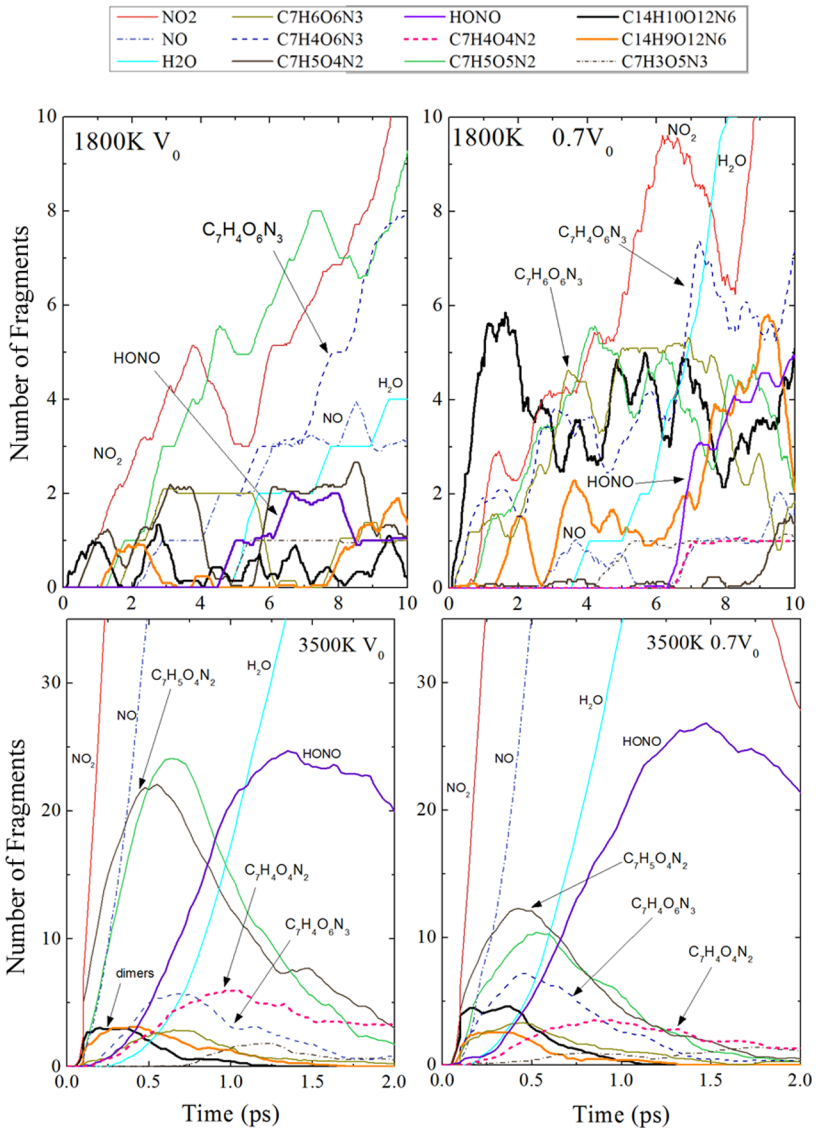

Figure 2. Initial decomposition intermediates in the thermal decomposition of condensed phase TNT at noncompressed (V_0) and 30% precompressed super cell (0.7 V_0).

of sublimation for energetic materials such as PETN, TATB, NM, and RDX compared to experimental results. The new energy term introduced is the low-gradient energy term of the form:

$$E_{lg} = -\sum_{ij,i<j}^{N} \frac{C_{lg,ij}}{r_{ij}^6 + R_{e_{ij}}^6} \tag{3}$$

Where r_{ij} is the interatomic distance, $R_{e_{ij}}$ is the interatomic equilibrium vdW distance, and $C_{lg,ij}$ is the dispersion energy correction parameter for the atomic pair i and j. Although no TNT-specific training was performed, we have ensured that major single molecule unimolecular decomposition pathways and energetics are reproduced with high accuracy compared to previously reported DFT results[30,36,37] indicating the applicability of the ReaxFF-*lg* force field to nitroaromatic (TATB, TNT) in addition to nitroaminic (RDX, HMX, NM) energetic materials. The obtained crystal density of TNT at ambient conditions was 1.49 gr/cm^3 compared to the experimental density of 1.65 gr/cm^3. The deviation is due to insufficient training of the *lg* parameters for TNT and has a negligible effect on the reported results. This can be deduced from the activation energies for V_0 (d = 1.49 gr/cm^3) and 0.9 V_0 (d = 1.65 gr/cm^3) super cells and the high similarity between the obtained intermediate and final species distributions during the simulations at the two densities (not shown).

2.2. Reactive Molecular Dynamics of TNT at Extreme Conditions. An initially noncompressed (V_0) super cell of 288 molecules (6048 atoms) was generated using an orthorhombic TNT unit cell (see Figure 1) obtained from the Cambridge Structural Database (database code CSD ZZZMUC01) available at the CCDC (http://www.ccdc.cam.ac.uk). The super cell was created by multiplying the a, *b*, and *c* cell vectors by 3, 6, and 2, respectively, to form a cubic shaped cell. Energy minimization using the conjugate gradient method was employed until convergence of potential energy was reached. Subsequent thermalization with a Berendsen thermostat at 300 K for 5 ps using a 25 fs damping constant was carried out to thermalize the system at room temperature. In order to relax excess pressure another 5 ps of isobaric−isothermal (NPT) relaxation was performed using a Nose-Hoover barostat at 1 atm and 300 K with 50 fs and 250 fs damping constants for temperature and pressure, respectively. By the end of this stage we have obtained the relaxed initial super cell (with $V_0 = 7.2 \times 10^3$ Å^3 and crystal density of 1.49 gr/cm^3). This initial super cell was used to generate the volumetrically compressed super cells. By shortening lattice parameters with fixed fractional coordinates for each compressed super cell we have obtained the 0.9 V_0, 0.8 V_0 and 0.7 V_0 super cells corresponding to 10%, 20%, and 30% compression. To further decrease any artificial stress caused by the method chosen to compress the cells, the group of compressed

dx.doi.org/10.1021/ja410020f | J. Am. Chem. Soc. 2014, 136, 4192−4200

super cells was energy minimized and further evolved through the microcanonical ensemble (NVE) for an additional 5 ps to obtain a fully relaxed set of super cells to be used in the decomposition simulation.

Target temperatures of 1800, 2250, 2500, 3000, and 3500 K were reached by rescaling the atomic velocities in a timespan of 100 fs. A Berendsen thermostat was imposed during the remainder of the simulation to maintain a constant temperature. This heating scheme results in an isothermal system and allows us to accurately extract Arrhenius parameters. Simulation length varied in the range 80−400 ps depending on temperature. Lower temperatures needed longer simulation time to attain steady state. The time steps used during thermalization and the rapid heating steps were kept at 0.25 and 0.1 fs, respectively. A small time step is essential in reactive simulations where chemical transformations occur and the chemical bond's vibrational frequency is accounted for. During each simulation, bond formation and rupture events were monitored at every time step. Each possible atomic pair was assigned a different bond order cutoff value to properly identify chemical species (standard values in ReaxFF C/H/O/N high-energy simulations). Hence, each pair having a higher cutoff than the specified value is considered to be bonded. The full set of force field parameters and cutoffs can be found in the Supporting Information.

2.3. DFT Calculations. DFT calculations were used in this study to calculate accurate energies for the species involved in the decomposition sequence, as revealed by ReaxFF-*lg* simulations. The calculations were carried out using the Gaussian 09 package.[38] The PBE1PBE hybrid density functional (also known as PBE0)[39,39b] was used in conjunction with the Dunning correlation consistent polarized valence double ξ (cc-pVDZ) basis set.[40] The PBE1PBE functional yields reliable results and is manageable in computational time requirements for large molecular systems such as those discussed. The vibrational analysis of the structures was performed at the same level of theory in order to reliably characterize the optimized structures either as local minima or transition states. All calculated frequencies, zero point energies, and thermal energies correspond to harmonic approximation. Calculations of intrinsic reaction coordinates (IRC) using internal coordinates were performed in order to examine whether the transition states under consideration connect with the expected reactants and products. These calculations were performed for all the transition states at the PBE1PBE level of theory. The basis set used was the same as that used for the stationary point optimizations.

3. INITIAL DECOMPOSITION MECHANISMS

The basic mechanisms that govern gas phase TNT decomposition were elucidated recently using extensive DFT calculations.[30,36] It was suggested that only unimolecular reactions are kinetically accessible during the passage of a shock wave (~6900 m/s) through a characteristic length scale of a unit cell of TNT (10−20 Å)[41−43] and that ring fission starts after most of the attached substituents are removed.[19,44] Three major decomposition routes were proposed as initiating agents of detonation, depending upon temperature and pressure conditions:[30] (1) C-NO_2 homolytic cleavage followed by subsequent C-NO_2 steps forming eventually three $NO_{2(g)}$ molecules and a triradical intermediate ($C_7H_5O_4N_2$); (2) C−H attack on the nitro substituent to form 2,4-dinitro-anthranil (DNAn, $C_7H_3O_5N_3$) and water; and (3) nitro-nitrite (C-NO_2 → C-ONO) rearrangement followed by O-NO homolytic cleavage and release of $NO_{(g)}$ for each of the three NO_2 substituents. It was suggested that above 1700 K the dominant pathway is a C-NO_2 homolytic cleavage, while other pathways are negligible.

In this study, we assess the influence of the bulk environment on the thermal decomposition. ReaxFF-*lg* simulations were carried out at temperatures in the range 1800−3500 K for super cells precompressed by 0−30% (V_0 − 0.7 V_0) incorporating periodic boundary conditions. Figure 2 shows the time evolution of the major species during the initial TNT decomposition for low- and high-temperature and pressure conditions. The full time evolution of main species is shown in Figure S1.

Figure 2 shows that the most dominant step of decomposition in all temperatures and compressions considered is a cleavage of the NO_2 substituent with production of the highly reactive $C_7H_5O_4N_2$ radical in agreement with DFT calculations.[30] We also find the di- and triradicals formed following the second and third NO_2 cleavages though in a smaller amount (not shown for clarity). NO radicals begin to appear concurrently with the formation of the $C_7H_5O_5N_2$ (TNT-NO) radicals. According to DFT and ReaxFF-*lg* calculations both routes become more exergonic at high temperatures. Water molecules and 2,4-dinitro-anthranil ($C_7H_3O_5N_3$) appear as products at a later stage and evolve at a slower rate.

ReaxFF-*lg* simulations predict formation of covalent TNT dimers very early in the decomposition with increasing amounts and rates for increased compressions. Various other radicals are produced during the initial decomposition steps, for example, the bimolecular formation of TNT radicals lacking a hydrogen atom ($C_7H_4O_6N_3$) and some with an extra hydrogen atom ($C_7H_6O_6N_3$). We also observe the unimolecular HONO elimination path leading to $C_7H_4O_4N_2$ at higher temperatures; however, it occurs at a slightly later stage and with a relatively low intensity. It is clear that the initial stage of thermal decomposition of condensed phase TNT involves a complex set of reactions the most significant of which are bimolecular.

4. STABLE GASEOUS PRODUCTS IN THE CONDENSED PHASE DECOMPOSITION

The final quantities of the stable gases, normalized by the initial number of TNT molecules, are shown in Figure 3. Both N_2 and

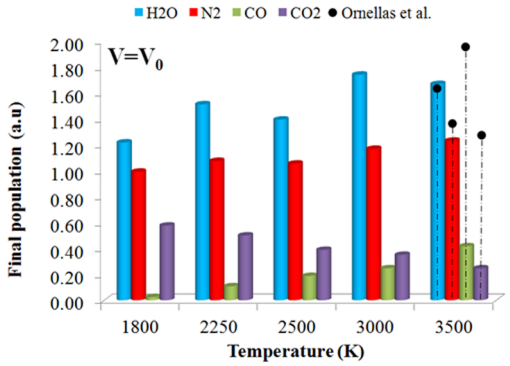

Figure 3. Normalized populations of stable final detonation gases.

H_2O are relatively insensitive to the wide range of applied temperature and compression values, while the combustion gases, CO and CO_2, seem to behave differently. As temperature increases the amount of CO_2 diminishes, while more CO is produced. We also noticed that higher compressions reduce the production of these gases, suggesting that oxygen is trapped in carbon clusters. Generally, higher temperatures and compressions enhance the production rate of all species. A detailed kinetic study will be presented in Section 5.

We compare the final populations for T = 3500 K and d = 1.49 gr/cm^3 ($V = V_0$), where most secondary reactions reached

dx.doi.org/10.1021/ja410020f | J. Am. Chem. Soc. 2014, 136, 4192−4200

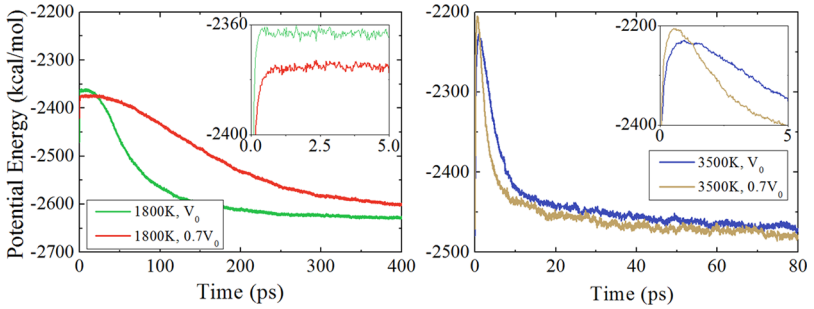

Figure 4. Thermal decomposition potential energy curves for lowest (1800 K) and highest (3500 K) temperatures for noncompressed (V_0) and 30% compressed (0.7 V_0) TNT.

a steady state, to available experimental results of calorimetric bomb experiments[45] of TNT with a density d = 1.53 gr/cm^3 conducted in vacuum confined environment. Post-detonation analysis identified the main detonation gaseous species to be N_2, H_2O, CO, and CO_2 with relative amounts of 1.32, 1.60, 1.98, and 1.25, respectively. The MD data show that the N_2 and H_2O produced in the MD simulation agrees well with the corresponding experimental values, however, CO and CO_2 deviate quite notably. One should be aware that the experimental measurements of detonation products are performed after isentropic expansion and subsequent cooling of the released gases, whereas our results are obtained in NVT ensemble conditions which characterize the reaction zone of the detonation wave. We assume that by performing an additional expansion of the systems a higher degree of combustion will be achieved, as was also found in other studies.[46,35] Moreover, nitroaromatic explosives such as TNT and TATB are known to produce large quantities of soot and carbonaceous clusters. Their evolution and thermodynamic analysis of carbon clusters will be discussed in a separate publication.

5. KINETICS AND THERMODYNAMICS OF DECOMPOSITION

The variation of potential energy of the system during the simulation is related to the thermal changes occurring during the decomposition process.[8,46,35] Hence, evidence for endothermic (seen in insets of Figure 4) and exothermic stages is clearly noticeable. The time evolution of the potential energy for the various systems examined is shown in Figure 4.

Inspection of Figure 4 reveals that in all cases the first stage in the decomposition process is endothermic. This stage corresponds to energy transfer from translational into vibrational modes of TNT molecules. This is followed by the start of the decomposition that involves bond rupture. The maximum value obtained in the potential energy profile marks the commencement of exothermic reactions and the formation of a large variety of intermediate species and final products together with energy release. The time dependence of the potential energy profile starting at the potential energy maximum is fitted to a decaying exponential function $U(t; T, P)$ used to extract kinetic and thermodynamic parameters of the exothermic stage in the decomposition process. The exponential function used for the fitting is shown in eq 4:[8]

$$U(t;\ T,\ P) = U_0 + \Delta Q \cdot \exp\left\{-\frac{t - t_{max}}{\tau_{exo}}\right\} \quad (4)$$

In eq 4 U_0 is the asymptotic potential energy of the system (kcal/mol), ΔQ is the exothermicity (cal/g), τ_{exo} is the inverse reaction rate (ps), and t_{max} (ps) is the time when the maximum in potential energy is obtained ("induction time"). To extract the global endothermic reactions rate constant (τ_{endo}), a first-order rate model (eq 5) was fitted to the TNT decomposition curves (Figure 3) from t = 0 up to $t = t_{max}$, where N_0 is the initial amount of TNT molecules. The quality of the fit was high (R^2 > 0.99), and it indicates a dominant unimolecular channel during the period between t = 0 and $t = t_{max}$. However, as will be demonstrated below, the decomposition of TNT in the condensed phase follows bimolecular reactions which subsequently promote the C-NO_2 unimolecular cleavage. The parameters obtained in these fits are presented in Table S1.

$$N(t) = N_0 \cdot \exp\left\{-\frac{t}{\tau_{endo}}\right\} \quad (5)$$

We observed that temperature variation plays a major role in the kinetics of both stages. The rate of the exothermic stage becomes 40 times faster for the noncompressed case when temperature is increased from 1800 to 3500 K, and an 80-fold faster kinetics is observed for the endothermic stage of TNT decomposition. Compression of the bulk has also a significant effect. For example, 20% volumetrically compressed TNT exhibits a 60% faster exothermic product evolution at 1800 K, suggesting that both stages in TNT decomposition are pressure dependent in the compression range examined and indicate a global bimolecular behavior. Similar behavior was also observed in the case of liquid TNT.[37] The calculated heat released during the exothermic step of compressed crystals, ΔQ, varies in the range 1091.7−1606.7 cal/g, where for a density of d = 1.49 gr/cm^3 ($V = V_0$) it is in the range 1091−1304 cal/g. Experimental data yield ΔQ values in the range 900−930 cal/g[47] (for d = 1.605 g/cm^3, T = 500−600K), 950 cal/g[48] (for d = 1.654 g/cm^3 T = 470−600 K), and 1082−1128[45] cal/g for d = 1.66 gr/cm^3 in vacuum confined experiments. These values are in good agreement with our results.

To investigate temperature and pressure dependence of the rate constant one can consider the total differential:

$$d\ln\ k\left(-\frac{\partial \ln\ k}{\partial T}\right)_P dT + \left(-\frac{\partial \ln\ k}{\partial P}\right)_T dP \quad (6)$$

The partial derivatives are evaluated using the first law of thermodynamics, $H = dU + pdV + Vdp$, together with the Arrhenius relation[49] $k = Ae^{-(E_a/RT)}$:

dx.doi.org/10.1021/ja410020f | J. Am. Chem. Soc. 2014, 136, 4192−4200

$$\left(\frac{\partial \ln\ k}{\partial\left(\frac{1}{T}\right)}\right)_P = -\frac{E_a}{R}; \quad \left(\frac{\partial \ln\ k}{\partial P}\right)_T = -\frac{\Delta V^{\ddagger}}{RT} \tag{7}$$

According to eq 7, an increase in pressure results in faster reaction rates only if the change in activation volume is negative. Conversely, a positive change in activation volume implies a decrease in the reaction rate for increasing pressure. Hence, a unimolecular reaction is expected to have a positive change in activation volume, while a bimolecular reaction is expected to exhibit a negative activation volume.[50,51]

Plotting the logarithm of the inverse reaction rate as a function of average pressure, one can extract the volume of activation, $\Delta V^{\ddagger}$, from the slope. The calculated average pressures for each compression and temperature and the calculated activation volumes are presented in Table 2.

Table 2. Average Pressures and Volumes of Activation during Decomposition

	average pressure (GPa) 1800 K		average pressure (GPa) 2500 K	
V_0	3.04		4.29	
0.9 V_0	4.38		5.94	
0.8 V_0	6.70		8.28	
0.7 V_0	10.53		13.04	
$\Delta V^{\ddagger}$ (cm^3/mol)	endo	exo	endo	exo
	−1.94	−2.69	−2.55	−1.66

As can be seen in Table 2 all changes in activation volumes are negative, as is expected from the decreasing magnitudes of the inverse rate constants for increasing compression. The rate constants for both endothermic and exothermic stages represent a complex mixture of many reactions that occur simultaneously. According to the calculated values of $\Delta V^{\ddagger}$ both stages are (at least) bimolecular in contrast to previous DFT and experimental results where a unimolecular rate-determining step was suggested for the initial endothermic stage. We could not find any experimental measurements of activation volumes of TNT, however, some data are reported for HMX, RDX, and nitromethane.[9,52,53] These are −5.6 cm^3/mol for α-RDX (at 478−508 K and 1.3−2.1 GPa), +3.89 cm^3/mol for β-RDX (at 508 K and 3−7 GPa), and +4.1 cm^3/mol (for β-HMX at 558−573 K and 3−8 GPa). Nitromethane exhibits complex kinetics with several pressure-dependent mechanism changes[8,54,55] and includes both positive and negative volumes of activation.[56] Our calculated values seem close in magnitude to the reported values of nitramine explosives and suggest that the global condensed phase TNT thermal decomposition is largely a bimolecular process. This finding is also supported by the initial decomposition stages presented in Figure 2 where dimerization and radical formation reactions are found to occur concurrently with NO_2 cleavage. Recently, Zhang et al,[46] used ReaxFF to study the thermal decomposition of both β-HMX and TATB. They found that both TATB and β-HMX decompositions are pressure dependent in the range 0−50% compression. Increasing pressure resulted in a decreased rate of β-HMX decomposition but led to an increase in the decomposition rate of TATB. Since TATB and TNT are structurally similar, one would expect them to behave similarly, as is found here. The activation energies for the endothermic and exothermic stages of the decomposition process were calculated and are presented in Figure 5.

The ReaxFF-*lg* predicted activation energies are in excellent agreement with experimental values. Nevertheless, there is a clear discrepancy in the values of the pre-exponential factors, which are up to 2 orders of magnitude larger in the simulations (units: s^{-1}) in comparison to the low-temperature measurements. We note, however, that our prefactors are in agreement with values reported by McGuire et al.[16] and Tarver et al.[47] in thermal explosion studies and with Zhang[46] in a ReaxFF thermal decomposition study of TATB, a similar high explosive.

The different measurement methods and experimental set ups together with variation in sample preparation and purity introduce large differences between the results. This sensitivity is not surprising considering the radical chain reaction mechanism. Scatter in the values of the pre-exponential factor could be related to the drastic temperature and diagnostic differences in different experimental set-ups. This variation between data obtained in different experiments, as seen in Figure 5, can lead to differences of up to 2 orders of magnitude in the value of the pre-exponential factor.[27] It is also worth mentioning that microstructure and purity of batches have a considerable effect on the prefactor. For instance, it was found that 2−10% of impurities in a TNT sample monotonically decrease the exponential prefactors up to almost 2 orders of magnitude compared with the values obtained for a pure sample.[57] Thus, it is not surprising that our results for a pure perfect single crystal exhibit larger prefactors. In addition, the decomposition is a radical mediated mechanism, thus it is

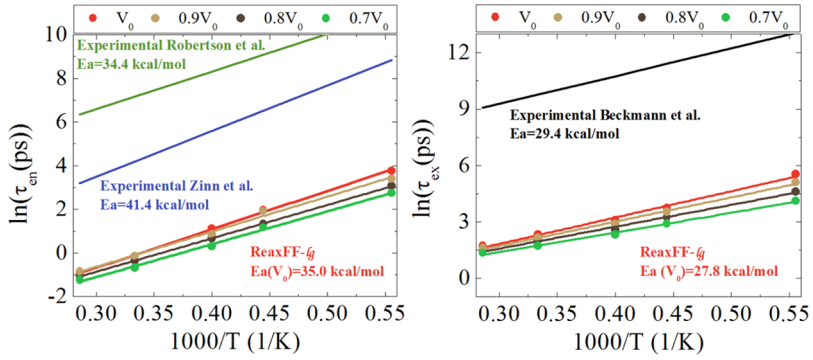

Figure 5. Arrhenius plots (τ = 1/k) for the endothermic (left) and exothermic stages (right) of decomposition at different compressions. Extrapolations for experimental results of Robertson et al.[6] (548−583 K EG study), Zinn et al[18] (571−763 K TTX study), and Beckmann et al.[28] (518−542 K IDSC study) are also shown.

dx.doi.org/10.1021/ja410020f | J. Am. Chem. Soc. 2014, 136, 4192−4200

extremely sensitive to radical quenching and subsequent inhibition by impurities.

The slopes of the linear regression analysis in Figure 5 allow us to extract the activation energies for the stages of the decomposition process at each material compression. These values are summarized in Table 3.

Table 3. Activation Energies and Pre-Factors for Both Stages of TNT Thermal Decomposition

stage	super cell	E_a (kcal/mol)	ln[A (s^{-1})]
endothermic	V_0	35.0	33.6
	0.9 V_0	32.0	33.1
	0.8 V_0	30.4	33.1
	0.7 V_0	29.9	33.2
Zinn et al.		**41.4**	**30.4**
Robertson et al.		**34.4**	**26.3**
exothermic	V_0	27.8	30.0
	0.9 V_0	25.7	29.8
	0.8 V_0	23.1	29.5
	0.7 V_0	20.7	29.3
Beckmann et al.		**29.4**	**22.8**

The activation energies represent an effective rate-limiting step for both the endothermic and exothermic stages of TNT decomposition. There is good agreement between the calculated activation energies and the experimental data from different sources and measurement methods. However, DFT calculations for a single TNT molecule unimolecular decomposition and laser powered homogeneous pyrolysis measurements on gas phase nitrobenzenes predicted for C-NO_2 bond rupture an activation energy which is higher by ~23 kcal/mol[30,36,5] than the condensed phase values described above. Inspection of Figure 2 clearly shows that the initial stage of TNT decomposition involves a dominant NO_2 production, as predicted by the DFT calculation. In this case, the difference in the predicted activation energies is puzzling. Moreover, the negative $\Delta V^{\ddagger}$ values obtained above suggest that a bimolecular mechanism is responsible for the endothermic stage, in contradiction with DFT predictions and some experimental findings. An analogous behavior is also observed for TATB, a similar nitroaromatic explosive: Some of the reported activation energies for a single molecule of TATB (C-NO_2 bond dissociation energy) lie in the range 69.4−77.2 kcal/mol,[11,12] while reported activation energies in the condensed phase lie in the range 42.0−60.0 kcal/mol.[16] In contrast, for RDX, HMX, and PETN, three high explosives representing nitramine and nitrate ester classes, the gas and condensed phases exhibit the same activation energy. Surprisingly, TNB is also characterized by similar activation energies in both gas and condensed phases. These findings, which to the best of our knowledge have never been addressed before, set apart some nitroaromatic energetic materials from all other organic explosives and are addressed here. The data of activation energies for a variety of systems is presented in Table 1.

6. DETAILED MECHANISM OF DECOMPOSITION

Thermal decomposition in the condensed phase results in formation of a large variety of radical fragments during the initial decomposition steps, some via bimolecular pathways. In turn, these radicals can promote further decomposition in a chain-like reaction. In contrast, in gas phase decomposition, formation of radical intermediates occurs to a much lesser extent. The ReaxFF-*lg* simulations presented above revealed that a major intermediate radical species is a TNT molecule lacking one hydrogen atom ($C_7H_4O_6N_3$) on the aromatic ring or on the methyl group, as can be seen in Figure 2. These species are produced very early in the decomposition, reach a maximum value, and then decrease to zero, as these radicals are rapidly consumed by the decomposition process. Thus, we focus on the interplay between bi- and unimolecular channels that are responsible for the experimental and our theoretical findings, namely, the reduced activation barrier for initial decomposition and the resulting facilitated C-NO_2 cleavage.

The reactive dynamics simulations demonstrate that the decomposition sequence in the condensed phase begins with an intermolecular hydrogen transfer between two adjacent TNT molecules. DFT calculations reveal that the hydrogen transfer that corresponds to the lowest energy path originates from the methyl group of one TNT molecule to one of the nitro groups on the other TNT molecule to form two radicals. In the following, we shall denote them by TNT_{-H} and TNT_{+H}, respectively. This initial event requires overcoming an energy barrier of 43.0 kcal/mol, much lower than the activation energy required for the unimolecular C-NO_2 cleavage (61.7 kcal/mol).

Once the two radicals were generated, each can further decompose. The $\bullet CH_2$ radical on TNT_{-H} can induce the transfer of a ring bound hydrogen to reconstruct the methyl group. This event is more likely to proceed via a lower energy bimolecular path ($\Delta E^{\ddagger}$ = 28.8 kcal/mol, ΔE = 27.1 kcal/mol) rather than from the higher energy unimolecular path (Scheme S1). The resulting radical vacancy on the ring has a marked influence on the energetic requirement for C-NO_2 cleavage: the *ortho* C-NO_2 bond dissociation energy is found to be ~23 kcal/mol lower (38.3 kcal/mol) than the corresponding value for an intact TNT molecule in the gas phase. The abstraction of ring bound hydrogen promotes breaking the adjacent C-NO_2 bond due to the formation of a new C≡C *cis* benzyne-type bond. This energy requirement is very close to the reported experimental values and to the result of our ReaxFF-*lg* calculations (29.9−35.0 kcal/mol).

TNT_{+H} can lead to the formation of HONO together with 2,4-dinitrotoluene radical ($C_6H_2(NO_2)_2CH_3^{\bullet}$), that we shall denote by TNT_{-NO_2}, via two transition states ($\Delta E^{\ddagger}_{TS2}$ = 38.0 kcal/mol and $\Delta E^{\ddagger}_{TS3}$ = 42.3 kcal/mol). Clearly, the vacancy formed by the missing NO_2 group can induce an intramolecular hydrogen transfer from the methyl group or an intermolecular transfer from a neighboring TNT molecule. The bimolecular route will lead to the formation of another TNT_{-H} radical if the hydrogen transfer is from the methyl group or to a TNT radical in which one of the aromatic hydrogen atoms is missing. The intramolecular route is accompanied by the release of 22.7 kcal/mol, while the intermolecular option requires overcoming a barrier of 10.9 kcal/mol to form a TNT radical with a missing ring bound hydrogen or a barrier of 3.0 kcal/mol to form the TNT_{-H} radical (Scheme S2). Thus, the generation of NO_2 and subsequently the thermal decomposition of TNT can be regarded as an autocatalytic event. This paves the way for major production of NO_2 radicals via bimolecular assisted channels all of which have a lower activation energy compared to the unimolecular route.

Two additional decomposition routes were identified accounting for other intermediates found in the simulations (Figure 2), all of them with significantly lower activation

dx.doi.org/10.1021/ja410020f | J. Am. Chem. Soc. 2014, 136, 4192−4200

barriers compared to the gas phase rupture of a C-NO_2 bond. TNT_{+H} can decompose via two different routes: The first, as already mentioned, yields HONO and 2,4-dinitrotoluene radical ($C_6H_2(NO_2)_2CH_3^{\bullet}$). The other route produces NO and 4-methyl-4,5-dinitrophenol ($C_6H_2(NO_2)_2(OH)CH_3$) with a barrier of 45.4 kcal/mol. The TNT_{-H} species can also decompose to generate NO and $C_6H_2(NO_2)(O)CH_2$ with a slightly higher barrier ($\Delta E^{\ddagger}_{TS5}$ = 47.7 kcal/mol). Thus, all the transition states involved in these decomposition paths require 20−28 kcal/mol less energy than the homolysis of C-NO_2 from a TNT molecule. A detailed description of the above routes is presented in Schemes S1−S3.

It is emphasized that the very first route of intermolecular hydrogen transfer is only possible if hydrogen atoms are available on the ring substituents (i.e., $-CH_3$, $-NH_2$), since the cleavage of a ring bound hydrogen requires much more energy. Hence, although TNB is an aromatic explosive very similar to TNT and TATB, its initial decomposition route is not likely to proceed via the bimolecular mechanism due to the high energetic cost of cleaving a ring bound hydrogen. Instead, TNB initial decomposition steps will proceed primarily by unimolecular C-NO_2 homolysis (weakest bond), as evidenced by similar activation energies for gas and condensed phases (Table 1).

For nonaromatic explosives, such as RDX and PETN, the decomposition proceeds via unimolecular channels, namely homolytic cleavage of the weakest bond ($\Delta E^{\ddagger}_{(O\text{-}NO_2)}$ = 46.5 kcal/mol and $\Delta E^{\ddagger}_{(N\text{-}NO_2)}$ = 41.5 kcal/mol, respectively). Therefore, bimolecular routes, as discussed above, including abstraction of hydrogen atoms and further NO_2 release become irrelevant. We verified this by a series of DFT calculations describing hydrogen transfer among two neighboring RDX molecules. It was found that the hydrogen transfer requires overcoming an energy barrier of 50.0 kcal/mol which is larger by 25% than the energy needed for unimolecular C-NO_2 bond rupture. This quantity is also larger by 25% than the energy required for the formation of a HONO product through intermolecular hydrogen transfer. These possible routes for RDX decomposition are described in Scheme S4. These results clearly indicate that in contrast to the initial decomposition steps of TNT and TATB that are dominated by a bimolecular hydrogen transfer assisted NO_2 production, nitramines and nitrate esters decomposition is expected to be dominated by unimolecular decomposition at the condensed phase.

It is interesting to compare these findings with possible contributions of ionic species to the decomposition process. Ionic species are expected to form at high temperatures as those used in the present study. Recently, Wang et al.[58] suggested that an intramolecular hydrogen transfer from CH_3 to an *ortho* NO_2 group in TNT is facilitated by ionization and leads to a decrease in activation energy of ∼20 kcal/mol. Thus, to assess the effects of ionization on the decomposition of TNT and other energetic compounds, we calculated the activation energy for the unimolecular C-NO_2 cleavage of various radical positive and negative species (see Table S3). We find that ionization of TNT lowers the C-NO_2 cleavage activation barrier by ∼27 kcal/mol, which is a similar energetic reduction as obtained in the routes discussed above. We also find that unlike TNT, the explosives RDX and PETN are prone to direct decomposition ($\Delta E^{\ddagger} \sim 0$ kcal/mol), following ionization except for a cationic RDX with $\Delta E^{\ddagger}$ = 19.4 kcal/mol. This implies that the aromaticity of nitroaromatic explosives maintains the stability of the ionic and neutral radical intermediates.

7. SUMMARY AND CONCLUSIONS

A comprehensive study based on ReaxFF-*lg* reactive molecular dynamics and DFT calculations revealed a universal principle in the mechanism of thermal decomposition of condensed phase nitroaromatic high explosives. The simulation scheme employing ReaxFF-*lg* reactive dynamics was validated with respect to DFT calculations and kinetic experiments. It was found that the decomposition of condensed phase TNT is pressure dependent, resulting in faster decomposition at higher pressures and leading to a negative volume of activation. Furthermore, the activation energy associated with thermal decomposition was found to be ∼35.0 kcal/mol, in excellent agreement to experimental measurements. This value is ∼20 kcal/mol lower than the calculated and experimental values for gas phase decomposition. Surprisingly, the enhanced reactivity toward decomposition is shared among other nitroaromatic high explosives. For instance, the activation energy for thermal decomposition of condensed phase TATB is lower by ∼19 kcal/mol than that expected for the unimolecular decomposition of a gas phase molecule. On the other hand, the activation energies for condensed phase TNB, RDX, and PETN are almost identical to those of unimolecular decomposition. The universal feature is an available hydrogen atom on the aromatic ring and on its substituents. The analysis shows that this behavior originates from a series of radical bimolecular reactions present in the condensed phase of nitroaromatic explosives. These reactions promote and sensitize the unimolecular C-NO_2 cleavage channel leading to the dramatically lower barrier for decomposition. Our findings suggest that the thermal decomposition of condensed phase nitroaromatic explosives, having available hydrogen atoms, is a bimolecular process. These results are in contrast to previous assumptions of unimolecular kinetics in the condensed phase and set apart the class of nitroaromatic explosives, as opposed to nitramines and nitrate esters, with regard to initial decomposition steps.

The crystalline structure is not essential for these bimolecular routes to be operational since liquid TNT exhibits very similar activation energy for thermal decomposition as the solid.[37]

■ ASSOCIATED CONTENT

Ⓢ Supporting Information

Additional information as noted in the text. This material is available free of charge via the Internet at http://pubs.acs.org.

■ AUTHOR INFORMATION

Corresponding Author

furman.david@mail.huji.ac.il

Notes

The authors declare no competing financial interest.

■ ACKNOWLEDGMENTS

S.V.Z. and W.A.G. were supported by the US ONR (N0014-12-1-0538 and N00014-09-1-0634). R.K. and Y.Z. acknowledge partial support of The Center of Excellence for Explosives Detection, Mitigation and Response, Department of Homeland Security.

REFERENCES

(1) Mochalin, V. N.; Shenderova, O.; Ho, D.; Gogotsi, Y. *Nature Nanotechnol.* **2012**, *7*, 11−23.
(2) Pichot, V.; et al. *Sci. Rep.* **2013**, *3*, 2159.
(3) Choi, W.; et al. *Nat. Mater.* **2010**, *9*, 423−429.
(4) Wu, C. J.; et al. *Nat. Chem.* **2009**, *1*, 57−62.
(5) Gonzalez, A. C.; Larson, C. W.; Mcmillen, D. F.; Golden, D. M. *J. Phys. Chem.* **1985**, *89*, 4809−4814.
(6) Robertson, A. J. B. *Trans. Faraday Soc.* **1948**, *44*, 977−983.
(7) Maksimov, Y. Y. *Zh. Fiz. Khim.* **1972**, *46*, 1726.
(8) Rom, N.; et al. *J. Phys. Chem. A* **2011**, *115*, 10181−202.
(9) Miller, P. J.; Block, S.; Piermarini, G. J. *Combust. Flame* **1991**, *83*, 174−184.
(10) Piermarini, G. J.; Block, S.; Miller, P. J. *Chem. Phys. Energ. Mater.* **1990**, *309*, 391−412.
(11) Rice, B. M.; S., S.; Owens, F. J. . *J. Mol. Struct.: THEOCHEM* **2002**, *583*, 69−72.
(12) Wu, C. J., Fried, L. E. First-Principles Study of High Explosive Decomposition Energetics. In Proceedings of the 11th International Detonation Symposium, Snowmass, CO, August 31−September 4, 1998; Office of Naval Research: Arlington, VA, 1998.
(13) Pexa, M.; Friedl, Z. *Cent. Eur. J. Energ. Mater.* **2010**, *7*, 131−144.
(14) Tarver, C. M.; Chidester, S. K.; Nichols, A. L. *J. Phys. Chem.* **1996**, *100*, 5794−5799.
(15) Rogers, R. N.; Janney, J. L.; Ebinger, M. H. *Thermochim. Acta* **1982**, *59*, 287−298.
(16) McGuire R. R., Tarver C. M. Chemical Decomposition Models for the Thermal Explosion of Confined HMX, TATB, RDX and TNT Explosives. In Proceedings of the 7th Symposium (International) on Detonation; Naval Surface Weapons Center NSWC MP, Annapolis, MD, June 16−19, 1981; Office of Naval Research: Arlington, VA, 1981; p 56.
(17) Satonkina, A. P. E. a. N. P. *Combustion, Explosion and Shock Waves* **2009**, *45*, 205−210.
(18) Zinn, J.; Rogers, R. N. *J. Phys. Chem.* **1962**, *66*, 2646−2653.
(19) Brill, T. B.; James, K. J. *Chem. Rev.* **1993**, *93*, 2667−2692.
(20) Cottrell, T. L.; Graham, T. E.; Reid, T. J. *Trans. Faraday Soc.* **1951**, *47*, 584−590.
(21) Ng, W. L.; Field, J. E.; Hauser, H. M. *J. Chem. Soc. Perk. T. 2* **1976**, 637−639.
(22) Lee, J. S.; Hsu, C. K.; Chang, C. L. *Thermochim. Acta* **2002**, *392*, 173−176.
(23) Tarver, C. M.; Tran, T. D. *Combust. Flame* **2004**, *137*, 50−62.
(24) Gibbs, R. T., Popolato, A. *LASL explosive property data*. University of California Press: Berkeley, CA, 1980.
(25) Minier, L. M.; Brower, K. R.; Oxley, J. C. *J. Org. Chem.* **1991**, *56*, 3306−3314.
(26) Davis, L. L.; Brower, K. R. *J. Phys. Chem.* **1996**, *100*, 18775−18783.
(27) Brill, T. B.; James, K. J. *J. Phys. Chem.* **1993**, 8759−8763.
(28) Beckmann, J. W.; Wilkes, J. S.; McGuire, R. R. *Thermochim. Acta* **1977**, *19*, 111−118.
(29) Stevenson, C. D. G.; P., M.; Batz, M. L. *J. Org. Chem.* **1996**, *61*, 5948.
(30) Cohen, R.; Zeiri, Y.; Wurzberg, E.; Kosloff, R. *J. Phys. Chem. A* **2007**, *111*, 11074−83.
(31) Liu, L.; et al. *J Phys Chem A* **2011**, *115*, 11016−22.
(32) Strachan, A.; et al. *Phys. Rev. Lett.* **2003**, *91*, 098301.
(33) Davis, L. L.; Brower, K. R. *AIP Conf. Proc.* **1998**, *429*, 699−702.
(34) Zhou, T. T.; Huang, F. L. *J. Phys. Chem. B* **2011**, *115*, 278−87.
(35) Strachan, A.; et al. *J. Chem. Phys.* **2005**, *122*, 54502.
(36) Chen, X.-F.; Liu, J.-F.; Meng, Z.-H.; Han, K.-L. *Theor. Chem. Acc.* **2010**, *127*, 327−344.
(37) Rom, N.; et al. *J. Phys. Chem. C* **2013**, *117*, 21043−21054.
(38) Frisch, M. J.; Trucks, G. W.; Schlegel, H. B.; Scuseria, G. E.; Robb, M. A.; Cheeseman, J. R.; Scalmani, G.; Barone, V.; Mennucci, B.; Petersson, G. A.; Nakatsuji, H.; Caricato, M.; Li, X.; Hratchian, H. P.; Izmaylov, A. F.; Bloino, J.; Zheng, G.; Sonnenberg, J. L.; Hada, M.; Ehara, M.; Toyota, K.; Fukuda, R.; Hasegawa, J.; Ishida, M.; Nakajima, T.; Honda, Y.; Kitao, O.; Nakai, H.; Vreven, T.; Montgomery, J. A., Jr.; Peralta, J. E.; Ogliaro, F.; Bearpark, M.; Heyd, J. J.; Brothers, E.; Kudin, K. N.; Staroverov, V. N.; Kobayashi, R.; Normand, J.; Raghavachari, K.; Rendell, A.; Burant, J. C.; Iyengar, S. S.; Tomasi, J.; Cossi, M.; Rega, N.; Millam, N. J.; Klene, M.; Knox, J. E.; Cross, J. B.; Bakken, V.; Adamo, C.; Jaramillo, J.; Gomperts, R.; Stratmann, R. E.; Yazyev, O.; Austin, A. J.; Cammi, R.; Pomelli, C.; Ochterski, J. W.; Martin, R. L.; Morokuma, K.; Zakrzewski, V. G.; Voth, G. A.; Salvador, P.; Dannenberg, J. J.; Dapprich, S.; Daniels, A. D.; Farkas, Ö.; Foresman, J. B.; Ortiz, J. V.; Cioslowski, J.; Fox, D. J., *Gaussian 09*, revision A.1; Gaussian, Inc.: Wallingford CT, 2009.
(39) (a) Perdew, J. P.; Burke, K.; Ernzerhof, M. *Phys. Rev. Lett.* **1997**, *78*, 1396−1396. (b) Adamo, C.; Barone, V. *J. Chem. Phys.* **1999**, *110*, 6158−6170.
(40) Dunning, T. H. *J. Chem. Phys.* **1989**, *90*, 1007−1023.
(41) Carper, W. R.; Davis, L. P.; Extine, M. W. *J. Phys. Chem.* **1982**, *86*, 459−462.
(42) Golovina, N. I.; Titkov, A. N.; Raevskii, A. V.; Atovmyan, L. O. *J. Solid State Chem.* **1994**, *113*, 229−238.
(43) Vrcelj, R. M.; et al. *Cryst. Growth Des.* **2003**, *3*, 1027−1032.
(44) Singh, G.; Kapoor, I. P. S.; Mannan, S. M.; Tiwari, S. K. *J. Hazard Mater.* **1999**, *68*, 155−178.
(45) Ornellas, D. L. *Calorimetric Determination of the Heat and Products of Detonation for Explosives*, Technical Report AD-A409329; UCRL-52821; Lawrence Livermore National Laboratory: Livermore, CA, 1982.
(46) Zhang, L.; et al. *J. Phys. Chem. A* **2009**, *113*, 10619−40.
(47) Tarver, C. M.; et al. *Symp. (Int.) Combust., [Proc.]* **1979**, *17*, 1407−1413.
(48) Wemhoff, A. P.; Hsieh, H. *TNT Prout-Tompkins Kinetics Calibration with PSUADE*, Technical Report UCRL-TR-230194; Lawrence Livermore National Laboratory: Livermore, CA, 2007.
(49) Eyring, H. *J. Chem. Phys.* **1935**, *3*, 107−115.
(50) Luft, G.; Recasens, F.; Velo, E. Kinetic properties at high pressure. In *High Pressure Process Technology: fundamentals and Applications*, Bertucco, A., Vetter, G., Eds.; Elsevier: Amsterdam, The Netherlands, 2001; Vol. *9*, pp 65−140.
(51) Jenner, G. *J. Phys. Org. Chem.* **2002**, *15*, 1−13.
(52) Bulusu, S. N. *Chemistry and Physics of Energetic Materials*; Kluwer Academic Publisher: Dordrecht, The Netherlands, 1990.
(53) Peiris, S. M. *Static compression of energetic materials*. Springer: New York, 2008.
(54) Piermarini, G. J.; Block, S.; Miller, P. J. *J. Phys. Chem.* **1989**, *93*, 457−462.
(55) Citroni, M.; et al. *J. Phys. Chem. B* **2010**, *114*, 9420−9428.
(56) Zeman, S.; Atalar, T.; Friedl, Z.; Ju, X.-H. *Cent. Eur. J. Energ. Mater.* **2009**, *6*, 119−133.
(57) Tran, T. D., Simpson, R. L., Maienschein, J., Tarver, C. M. *Thermal decomposition of trinitrotoluene (TNT) with a new one-dimensional time to explosion (ODTX) apparatus*, Technical Report UCRL-JC-141597; Lawrence Livermore National Laboratory: Livermore, CA, 2001.
(58) Wang, B.; et al. *J. Phys. Chem. A* **2011**, *115*, 8142−8146.